The ATLAS SCT grounding and shielding concept and implementation

R.L. Bates,[a] **P.J. Bell,**[b] **J. Bernabeu,**[c,1] **J. Bizzell,**[d] **J. Bohm,**[e] **R. Brenner,**[f]
P.A. Bruckman de Renstrom,[g] **A. Catinaccio,**[h] **V. Cindro,**[i] **A. Ciocio,**[j] **J.V. Civera,**[c]
S. Chouridou,[k] **P. Dervan,**[l] **B. Dick,**[m] **Z. Dolezal,**[n] **L. Eklund,**[b] **L. Feld,**[o] **D. Ferrere,**[b]
S. Gadomski,[b] **F. Gonzalez,**[c] **E. Gornicki,**[g] **A. Greenhall,**[l] **A.A. Grillo,**[k]
J. Grosse-Knetter,[p] **M. Gruwe,**[h] **S. Haywood,**[d] **N.P. Hessey,**[q] **Y. Ikegami,**[r] **T.J. Jones,**[l]
J. Kaplon,[h] **P. Kodys,**[n] **T. Kohriki,**[r] **T. Kondo,**[r] **S. Koperny,**[s] **C. Lacasta,**[c]
J. Lozano Bahilo,[t] **P. Malecki,**[g] **F. Martinez-McKinney,**[k] **S.J. McMahon,**[d]
A. McPherson,[h] **B. Mikulec,**[h] **M. Mikuž,**[i] **G.F. Moorhead,**[m] **M.C. Morrissey,**[d] **K. Nagai,**[u]
A. Nichols,[d] **V. O'Shea,**[a] **J.R. Pater,**[v] **S.J.M. Peeters,**[w] **H. Pernegger,**[h] **E. Perrin,**[b]
P.W. Phillips,[d] **J.P. Pieron,**[x] **S. Roe,**[h] **J. Sanchez,**[c] **E. Spencer,**[k] **J. Stastny,**[e]
J. Tarrant,[d] **S. Terada,**[r] **M. Tyndel,**[d] **Y. Unno,**[r] **R. Wallny,**[y] **M. Weber,**[z]
A.R. Weidberg,[aa] **P.S. Wells,**[h] **P. Werneke**[q] **and I. Wilmut**[d]

[a]*SUPA - School of Physics and Astronomy, University of Glasgow,*
Glasgow, United Kingdom

[b]*Section de Physique, Université de Genève,*
Geneva, Switzerland

[c]*Instituto de Fisica Corpuscular (IFIC), University of Valencia and CSIC,*
Valencia, Spain

[d]*Particle Physics Department, Rutherford Appleton Laboratory,*
Didcot, United Kingdom

[e]*Institute of Physics, Academy of Sciences of the Czech Republic,*
Praha, Czech Republic

[f]*Department of Physics and Astronomy, University of Uppsala,*
Uppsala, Sweden

[g]*The Henryk Niewodniczanski Institute of Nuclear Physics, Polish Academy of Sciences,*
Krakow, Poland

[h]*CERN,*
Geneva, Switzerland

[i]*Department of Physics, Jožef Stefan Institute and University of Ljubljana,*
Ljubljana, Slovenia

[1]Corresponding author.

^{j}*Physics Division, Lawrence Berkeley National Laboratory and University of California,*
  Berkeley CA, United States of America

^{k}*Santa Cruz Institute for Particle Physics, University of California Santa Cruz,*
  Santa Cruz CA, United States of America

^{l}*Oliver Lodge Laboratory, University of Liverpool,*
  Liverpool, United Kingdom

^{m}*School of Physics, University of Melbourne,*
  Parkville, Victoria 3010, Australia

^{n}*Faculty of Mathematics and Physics, Charles University in Prague,*
  Praha, Czech Republic

^{o}*RWTH Aachen University, I. Physikalisches Institut,*
  Aachen, Germany

^{p}*II Physikalisches Institut, Georg-August-Universität,*
  Göttingen, Germany

^{q}*Nikhef National Institute for Subatomic Physics and University of Amsterdam,*
  Amsterdam, Netherlands

^{r}*KEK, Oho 1-1,*
  Tsukuba, Ibaraki 305-0801, Japan

^{s}*Faculty of Physics and Applied Computer Science, AGH-University of Science and Technology,*
  Krakow, Poland

^{t}*Universidad de Granada and CAFPE,*
  Granada, Spain

^{u}*Institute of Pure and Applied Sciences, University of Tsukuba,*
  Ibaraki, Japan

^{v}*School of Physics and Astronomy, University of Manchester,*
  Manchester, United Kingdom

^{w}*Department of Physics and Astronomy, University of Sussex,*
  Brighton, United Kingdom

^{x}*Department of Physics, University of Wisconsin,*
  Madison WI, U.S.A.

^{y}*University of California,*
  Los Angeles, U.S.A.

^{z}*Karlsruhe Institute of Technology,*
  Karlsruhe, Germany

^{aa}*Department of Physics, Oxford University, Oxford,*
  United Kingdom

E-mail: Pepe.Bernabeu@ific.uv.es

ABSTRACT: This paper describes the design and implementation of the grounding and shielding system for the ATLAS SemiConductor Tracker (SCT). The mitigation of electromagnetic interference and noise pickup through power lines is the critical design goal as they have the potential to jeopardize the electrical performance. We accomplish this by adhering to the ATLAS grounding rules, by avoiding ground loops and isolating the different subdetectors. Noise sources are identified and design rules to protect the SCT against them are described. A rigorous implementation of the design was crucial to achieve the required performance. This paper highlights the location,

connection and assembly of the different components that affect the grounding and shielding system: cables, filters, cooling pipes, shielding enclosure, power supplies and others. Special care is taken with the electrical properties of materials and joints. The monitoring of the grounding system during the installation period is also discussed. Finally, after connecting more than four thousand SCT modules to all of their services, electrical, mechanical and thermal within the wider ATLAS experimental environment, dedicated tests show that noise pickup is minimised.

Contents

1 The ATLAS SCT

The ATLAS experiment [1] is one of two general-purpose detectors at CERN's Large Hadron Collider (LHC). The SemiConductor Tracker (SCT) is a silicon strip detector and forms the intermediate tracking layers of the ATLAS inner detector (figure 1).

The SCT is geometrically divided into a central barrel region and two endcaps (known as 'A' and 'C'). The barrel region consists of four concentric cylindrical layers (barrels). Each endcap consists of nine disks. The innermost and outermost radii of the barrel are 300 mm and 520 mm. The endcaps innermost and outermost radii are 275 mm and 560 mm.

Barrel layers consist of one single module type, arranged in rows [2]. The endcap disks consist of modules arranged in rings [3]. One disk can have up to three rings, and the endcap modules are
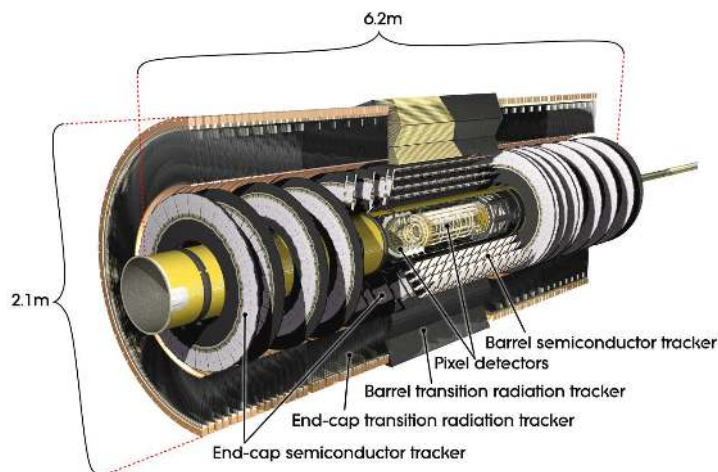
Figure 1. ATLAS Inner Detector. The SCT is within the Transition Radiation Tracker (TRT) and surrounds the Pixel detector. The SCT barrel has four layers and each of the endcaps has nine disks.

Figure 2. Picture of a barrel module (left). Three different types of endcap modules (right).

of three types: inner, middle (or short middles) and outer, corresponding to the different rings (figure 2).

The complete SCT consists of 4088 modules [4, 5]. Each module has two planes of silicon, each with 768 active strips of p^+ implant on n-type bulk [6]. The planes are offset by a small stereo angle (40 mrad), so that each module provides space-point resolutions of 17 μm perpendicular to and 580 μm parallel to its strips. The implant strips are capacitively coupled to aluminium metallization, and are read out by the front-end electronics located on a printed circuit board (known as a hybrid) on low-radiation-length material, which hosts twelve 128-channel ASIC chips (ABCD3TA [7]). The complete SCT has 49,056 front-end ASICs and more than six million individual read-out channels.

The SCT uses a "binary" readout architecture. For each channel, the signal is amplified, discriminated to one bit, stored in a digital pipeline memory and digitally read out. The only pulse-height information transmitted by the front-end chips is one bit per channel which denotes whether the pulse was above a preset threshold. Further information about the size of the pulse cannot be recovered later, so the attenuation of the electromagnetic interference is crucial to the successful operation of the detector.

The discriminator threshold must be set at a level that guarantees uniform good efficiency while maintaining the noise occupancy at a low level. Furthermore, the silicon part of the SCT detector must maintain good performance even after a total ionising dose of $100\,\mathrm{kGy}$, and a non-ionising fluence of $2\mathrm{x}10^{14}$ neutrons/cm^2 of $1\,\mathrm{MeV}$ neutrons equivalent corresponding to 10 years of operation of the LHC at its design luminosity. The physics performance requirements, based on track-finding and pattern-recognition considerations, are that single strip hit efficiency should be greater than 99% and noise occupancy less than $5\mathrm{x}10^{-4}$ per channel even after irradiation.

A minimum ionising particle generates approximately $3.6\,\mathrm{fC}$ charge in the $285\,\mu\mathrm{m}$-thick silicon detector. The charge is collected typically in one or two strips, typical strip pitch is $80\,\mu\mathrm{m}$. Each strip is connected to one input of the front-end chip. The signal is amplified and shaped to $20\,\mathrm{ns}$ peaking time and then discriminated by a single comparator. The noise level before irradiation is around $0.24\,\mathrm{fC}$. In order to meet the design specifications of high efficiency and low noise, the threshold is normally set to $1\,\mathrm{fC}$. This threshold is adjustable to allow good discrimination between signal and noise during the 10 years of operation.

Minimising the noise is essential to have a good discrimination margin and to achieve the required noise occupancy. Electromagnetic interference (EMI) occurring in the input path of the detector to the comparator appears as additional noise to that of the amplifier and detector. The grounding and shielding task is to attenuate EMI in the detector and front-end electronics before the discriminator.

The regions which are most susceptible to EMI are the silicon strip detector and its signal path to the amplifier, which includes the signal return path. This small-signal path will be described more fully in section 3.1.

If EMI attenuation design is sufficient, then the threshold increase to accommodate it should be less than 5%. Since the discriminator threshold is set at $\sim 1\,\mathrm{fC}$ of input signal charge, the detected EMI should require a threshold increase of less than $50\,\mathrm{aC}$ input equivalent.

By comparing single module noise levels with module array noise measurements, the total EMI induced noise can be estimated. The power and servicing cables extend radially from the tracker up to $120\,\mathrm{m}$ at all angles. The cables are in close proximity to most of the other ATLAS systems, so EMI from all other systems is difficult to estimate and control. Noise measurements have been taken as the SCT subsystems were assembled, verifying that system EMI should not compromise the detector performance. However, the actual EMI value can only be learned after designing and installing the entire ATLAS experiment, with all ATLAS subsystems operational.

The SCT detector, being part of the ATLAS experiment, is affected by mechanical and electrical constraints. Section 2 explains these constraints on the SCT grounding and shielding. The SCT grounding and shielding concept is described in section 3. To achieve the desired EMI attenuation, many standard techniques were employed in the power supply design, cabling, filters, detector shielding, bonding, and module design. Section 4 explains the implementation of the SCT grounding and shielding. During the fabrication and installation of the SCT several problems arose, they are described in section 5. Finally, section 6 concludes by explaining the performance of the grounding and shielding system.

2 The ATLAS context

2.1 Grounding and shielding policy

The ATLAS detector consists of many complex components, installed and operating in contiguous volumes, resulting in a large amount of installed equipment with multiple interconnections and shared services. For these reasons, if these issues are not properly taken care of already at the design stage and systematically followed up during installation, the performance of the detector components could be adversely affected by electromagnetic interference or induced electronic noise.

An ATLAS grounding and shielding policy was developed in the design phase of the experiment [8] to minimise possible electromagnetic interference effects. Large detector subsystems have many connections to the surrounding world for signals, monitoring, power, cooling, etc.; if left to chance, a bewildering network of ground loops will arise. Thus, apart from safety considerations, one of the main concerns has been the prevention of ground-loop currents that would couple to the signals of the detector systems.

The main guidelines of the ATLAS policy can be summarised in these rules:

- All detector systems are electrically isolated, which implies that there are no connections between different detector systems.

- Power supplies are floating.

- There are no connections to ground other than through the unique safety ground point.

- Each subdetector is located in a Faraday cage.

In addition, electromagnetic compatibility of ATLAS electronic equipments has been insured to achieve the expected level of performance of the experiment. The ATLAS electromagnetic compatibility policy [9] defined the electrical safety aspects of the electronic systems for a proper operation in the ATLAS electromagnetic environment.

2.2 The ATLAS caverns

In addition, the design of the SCT grounding and shielding has mechanical constraints. ATLAS is installed in an experimental cavern at 92 m depth (UX15), where LHC collisions occur. Power supplies, readout electronics, cooling and monitoring systems, etc. have been installed in two adjacent caverns, US15 and USA15, where there are much lower radiation levels and magnetic fields, allowing access for maintenance. In the service caverns, the development of special field-resistant electronics is unnecessary. Thus, the SCT electronic system spans a huge volume, with cables up to 120 m long between the detector and the service cavern electronics as shown in figures 3 and 4.

Modules on the same barrel cylinder or the same endcap are supplied from power supplies in both adjacent caverns. Furthermore, due to the complicated cable path inside the ATLAS detector, modules in the same detector array going to the same power-supply cavern can have very different cable paths. Very big loops with other subdetector electronics inside are formed (figure 5). This is unavoidable and the grounding and shielding design must minimise this big ground-loop effect. ATLAS line-voltage earth potentials in USA15, UX15 and US15 can vary because they are quite
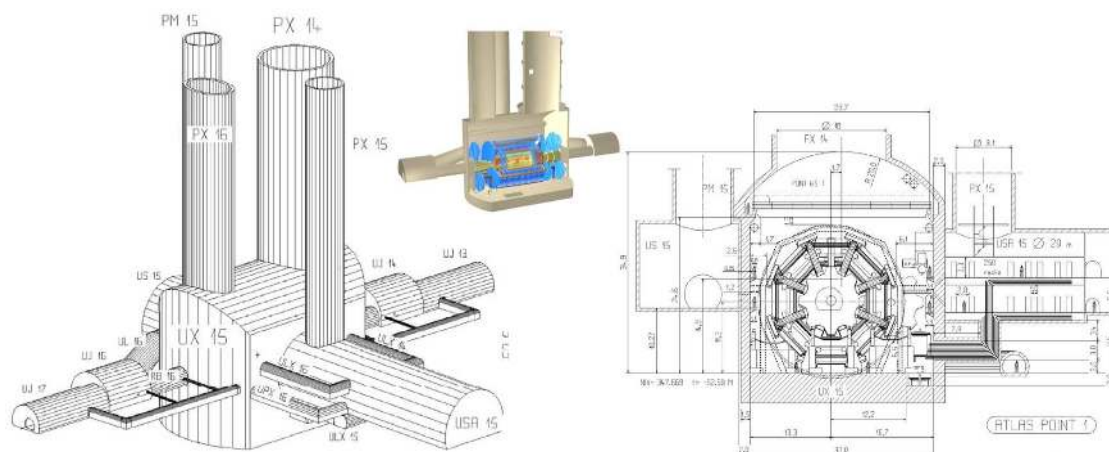
Figure 3. Schematic view of the underground ATLAS installation. The detector cavern is UX15, the adjacent service caverns are USA15 and US15. PX14 and PX16 are the installation shafts for surface access, PM15 and PX15 are the two elevators. The detector is almost as large as the UX15 cavern.
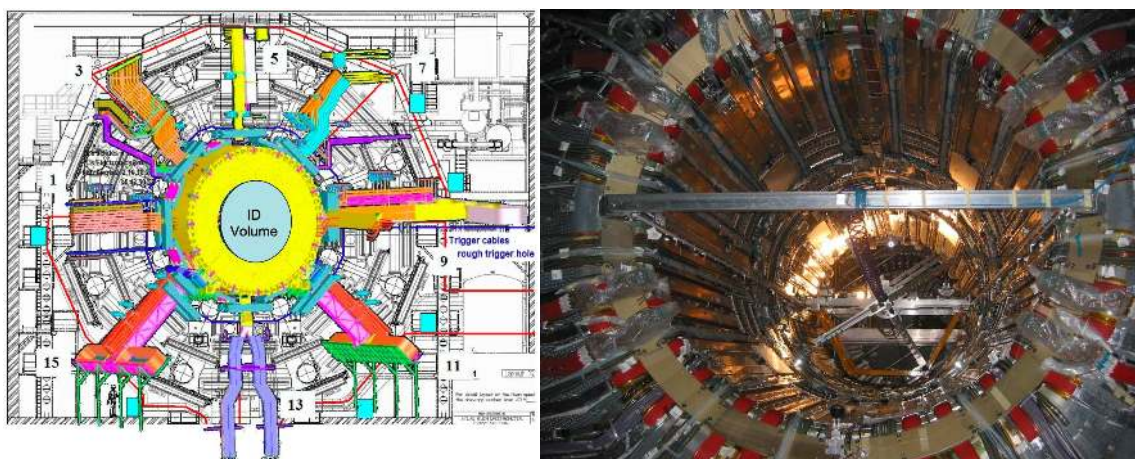

Figure 4. On the left, a cross-section of the ATLAS cavern UX15 (30 m wide and 35 m high, 50 m long). The SCT services arriving from the adjacent caverns are highlighted. The picture on the right is the Inner Detector (ID) volume before detector installation. Very careful packing of the various subdetector services is required in the constrained space, so that isolation of each subdetector shielding system can be guaranteed.

far apart. Following the ATLAS policy of having a single connection to ground; power-supply returns and cable shields are floating at the power-supply end in order to minimise ground loops at low frequencies through ATLAS grounds.

3 Grounding and shielding concept

The main role of the grounding and shielding concept is the prevention of electromagnetic interference or "noise pickup". It protects the SCT against external sources of noise and it also protects the SCT neighbour systems against the noise that it radiates. In the SCT, the most sensitive region
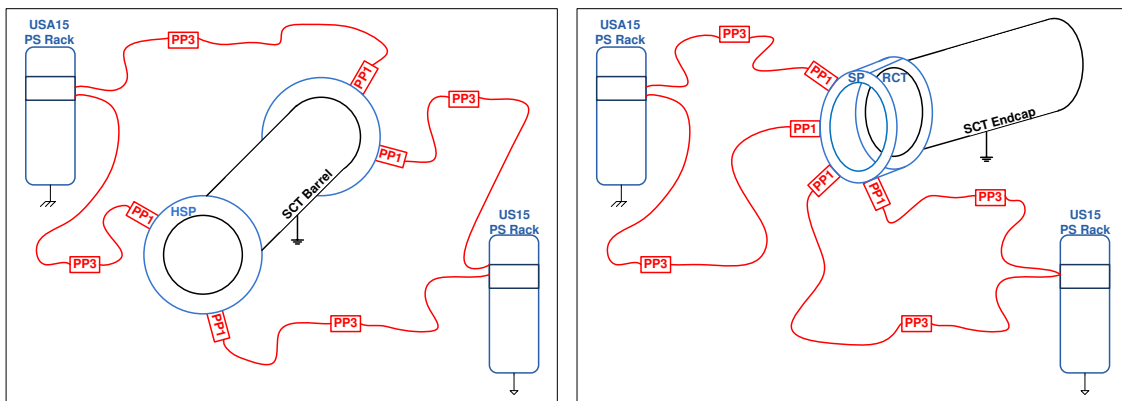
Figure 5. The module service cables are laid in widely separated paths throughout the ATLAS volume. Floating power supplies in the PS racks drive the cables, so the ground loops between cables are mostly completed by substantial distributed capacitance to earth over the cable paths. In the left-hand figure, the barrel detector sensors straddle the ground loop between the service cable arrays of Side A and Side C. In the right-hand figure, the endcap sensors are outside the service cable ground loops.

is the small-signal path between sensor and amplifier. There are several potential noise sources and means of transmission:

1. EMI from circuits generated locally at the sensor module or from adjacent modules.

2. Electromagnetic radiation from surrounding ATLAS detectors.

3. Conducted EMI currents through the module service cables or system shielding, captured primarily by ground loops.

4. EMI from the metal cooling tube to which each sensor module is clamped.

First, we will describe the small-signal path more fully. Next, we discuss the module design techniques to attenuate Source 1. A well-designed Faraday cage is the best means to reduce externally captured EMI, Source 2 and Source 3. Finally, we will comment on techniques that address Source 4, the cooling pipe relationship with the module.

3.1   Small-signal path

The EMI shielding design starts with the identification of the small-signal path. In the SCT, the small signal is generated in the depleted silicon sensor when an energetic particle crosses. The detector respresents a current source. The small-signal path is the entire current loop that the physics signal travels along to dissipate its energy.

As shown in figure 6, the small-signal path includes the silicon-strip diode and strip metal, the front-end chip amplifier, the hybrid analogue ground plane, and the detector high voltage (HV) backplane bias that is AC bypassed to the hybrid analogue ground. In addition, a pitch adapter and several bondwires are part of the path from detector to amplifier [4, 5]. EMI current induced into the small-signal path is indistinguishable from signal, since the binary readout does not permit a filtering scheme. The hybrid ground is the zero-volt reference for the small signal.
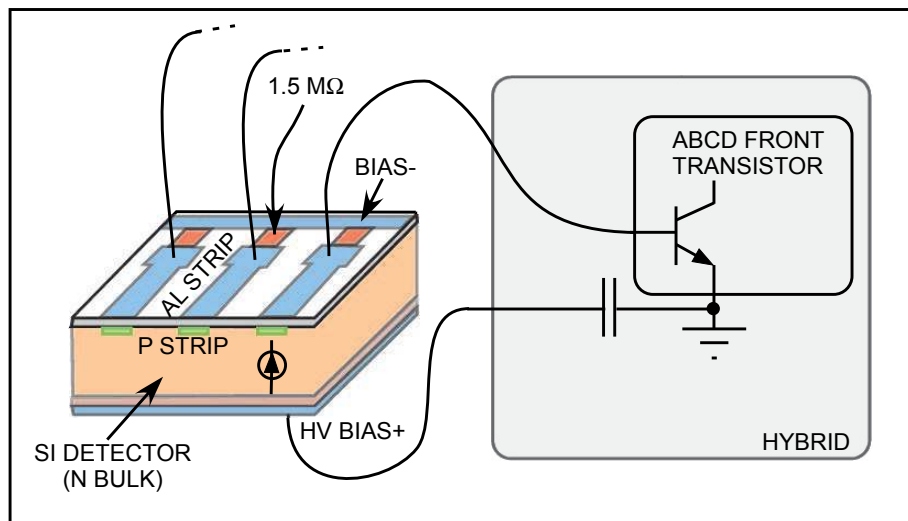
Figure 6. Small-signal path. The signal is generated in the silicon, routed from the strip to the amplifier in the chip. The return path includes the ground node at the chip and the hybrid, the HV capacitor and the detector backplane.

The small-signal ground is that part of the small-signal path that multiple strips have in common. Included in this sub-category of the small-signal path are the front-end chip internal analogue ground bus, the hybrid analogue ground, the detector-HV backplane, and their connecting wire-bonds. Most SCT EMI couples into the electronics at the small-signal ground since connection to the service-power return and digital section is essential. The front-end channels can also crosstalk through their common small-signal ground connection. A useful diagnostic model is to look for induced EMI currents through the small-signal ground.

Four design techniques are used to minimise EMI pickup in the small-signal path:

1. Make the small-signal ground as low resistance and low inductance as is practically possible. EMI currents in the small-signal ground appear as pickup voltages at the front-end preamplifier transistor. Minimising the small signal-ground impedance minimises the voltage at the front-end amplifier induced by an EMI current.

2. Reference the detector module at a single point, the power-supply connector, away from the small-signal ground. Supplementary connectors should be close to the power-supply connection. This single-point tie avoids placing the small-signal ground in the loop between two external conductors, which will usually have an AC potential across them.

3. On the hybrid, avoid the flow of currents from other services through the small-signal ground. Logic and optical drivers on the hybrid should have their own path to the power-supply connector, and the path should be as independent as practical from the small-signal ground.

4. Nearby conductors that are external to the module need to be shielded from the detector and small-signal paths. The stray capacitance to the external conductor forms a ground loop that includes the small signal path, the power return, and the referencing path between the power-supply return and the external conductor. The module-cooling tube couples to the detector
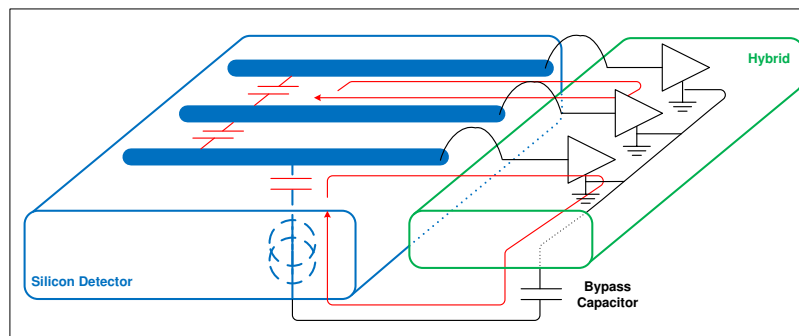
Figure 7. One magnetic loop antenna is comprised of a strip and its small-signal path returning through the detector backplane. A second loop occurs with the stray capacitance across two adjacent strips and their small-signal path to the chip ground bus. Both loop areas are small, and the radiated EMI susceptibility is modest.

sensor with $\sim$100 pF capacitance in the simplest configuration. This direct coupling is reduced using an electrostatic shield, called the shunt shield. Unattenuated, this capacitance would create an EMI loop through the small-signal path.

The detector module has low susceptibility to radiated EMI since the receiving antennae loop areas are small. Two loops are indicated in figure 7. The interstrip loop area is limited by the $\sim$80 μm strip pitch, and the strip-to-backplane loop area is limited by the detector thickness of $\sim$285 μm. On the other hand, the 12 cm long strips could receive electric field interferences. Thus, even if the susceptibility is low, the front-end electronic design should avoid local electromagnetic radiation that could couple to the sensitive amplifiers.

3.2 Faraday cage and power cables

As seen in the previous section, an isolated module has a fair EMI resistance even without a complete shield enclosure. However, in the SCT, the detector modules overlap each other by $\sim$2.5% of their area. Modules are about 6 cm wide and 6-12 cm long (figure 2), and overlap a few millimetres along each edge. In the overlap area, the sensors are $\sim$2 mm apart [10]. This parasitic capacitance to another sensor disturbs the small-signal path of the overlapping strips: overlapping sensors can have cables widely separated in the cavern. Thus, much of the EMI design is devoted to filtering the cable EMI, and reducing cable common-mode AC differences.

The primary purpose of the Faraday cage is to provide a low-impedance common-bonding node for the cable shields and cable-entry filters at PP1 (Patch Panel 1). In addition, the shield provides a common referencing point for all conductors inside, minimising the voltage difference between two internal parts (i.e. between two adjacent modules). Three main rules should be implemented:

- Every conductor entering the Faraday cage must be shielded.

- Every cable entering the cage has its shield bonded to the cage at its entry point.

- Every conductor going inside the cage should short to the cage skin or receive capacitor bypassing.
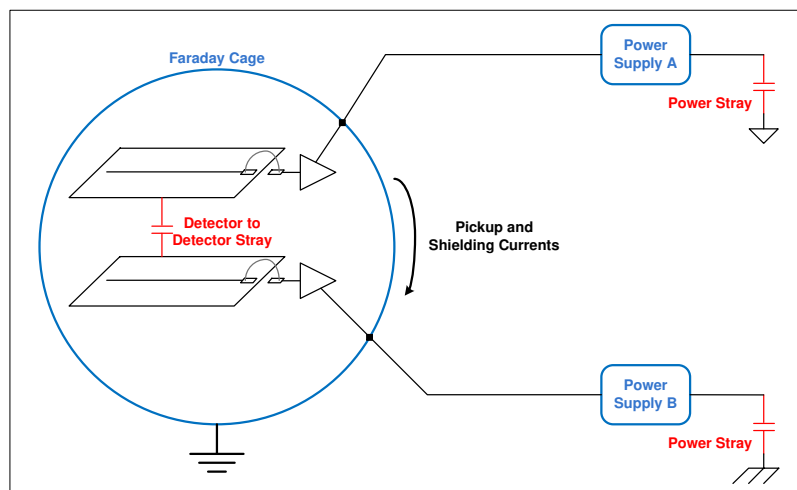
Figure 8. In the absence of the Faraday shield, noise currents would flow through the modules. The shield protects the modules from noise currents.

Figure 8 illustrates the ground loop resulting from the overlap of modules, and the action of the Faraday cage that shunts the loop. The tie to the ATLAS earth environment is completed by the distributed-shield stray capacitance of the long cable runs. Noise currents generated in the external-cable ground loop will be diverted through the Faraday cage, attenuating the noise-current entry into the module small-signal paths. The attenuation is directly dependent on the conductivity of the cage, which is dominated by the electrical bonding joints between the cage sections and the joints between the cage and the cable shields.

The main tool for reducing the EMI to the detector small-signal paths is designing a high conductivity skin. Also, the cage apertures should be minimised. Only one single tie from the Faraday cage to the safety earth should be used to avoid needless ground-loop currents in the enclosure walls.

A complete shield envelops each of the three parts of the SCT (Barrel and Endcaps A and C), each one having a single safety-earth cable. These three earth cables are tied to earth at the same point to minimise potential differences between the three detector parts.

Given the unavoidable ground loops shown in figure 5, filtering is essential. As explained later, the various power cables have different lengths and thicknesses. Filter networks occur at two patch panels, PP1 and PP3. The locations of PP1 and PP3 are detailed in sections 4.6 and 4.7. The cable shields are AC-coupled at the power supply to avoid DC currents in the cable shields. The barrel cage is included in the service-cable ground loop, so EMI shielding currents circulate along the barrel. The endcap cages are outside of their respective service-cable ground loops, and noise currents are probably modest on the endcap cages.

In both barrel and endcap, good radial connections between all PP1 shield nodes are needed, so as to reduce noise currents on the cage skin. In the case of the barrel, noise currents between the shields of cables arriving at each end of the barrel will flow along the barrel cage. Therefore, it is important that the resistance of the cage skin is minimal.
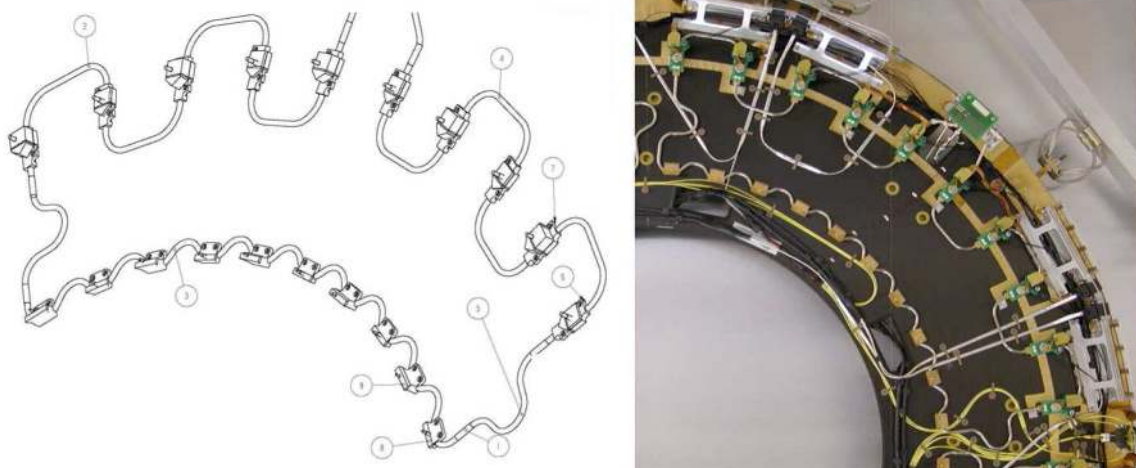
Figure 9. Module cooling tube on one quarter of an endcap disk. It forms a loop very close to the modules inside the Faraday cage.

3.3 Cooling loops

Each detector module is thermally coupled to a cupronickel evaporative-cooling tube that connects adjacent modules. The cooling tubes provide little useful EMI shielding function, but the shielding and bonding design must accommodate their high conductivity and large stray capacitance to the sensors.

A module cooling tube will enter and exit the Faraday cage at almost the same point in the cage (figure 9). The tube bonds to the cage at its entry and exit, so no isolation of the cooling tube is needed.

The cooling loops travel very close to the detectors, with large capacitance to the silicon detector sensor, so noise currents on the tubes must be minimised. Stray capacitance between a cooling tube and a detector sensor can be as large as 100 pF. Since the cooling tube serves modules, with power tapes entering the Faraday cage at very different points, the tube stray capacitance creates a ground loop that includes the detector sensors. The potential ground loop would include a cooling tube, its module sensors with different power supply groups, and the portion of the cage between the two power-supply entry points. Additionally, the service cable EMI from outside PP1 that PP1 does not filter will appear in the ground loop. This cooling ground-loop problem is more important in the barrel as cooling tubes serve modules that have power tapes entering at both ends of the barrel, so the loop area is large. A module shunt-shield between the cooling tube and the detector sensor is needed to minimise noise currents going through the detector sensor, thereby protecting the small-signal path. This shunt-shield is described in section 4.3.

4 Grounding and shielding implementation

As mentioned above, in the SCT, all supplies are floating following the ATLAS grounding policy. The barrel and two endcaps form three independent, isolated detector volumes with references to a single earth. Each volume has a complete shield skin with a single-earth safety-bond point.
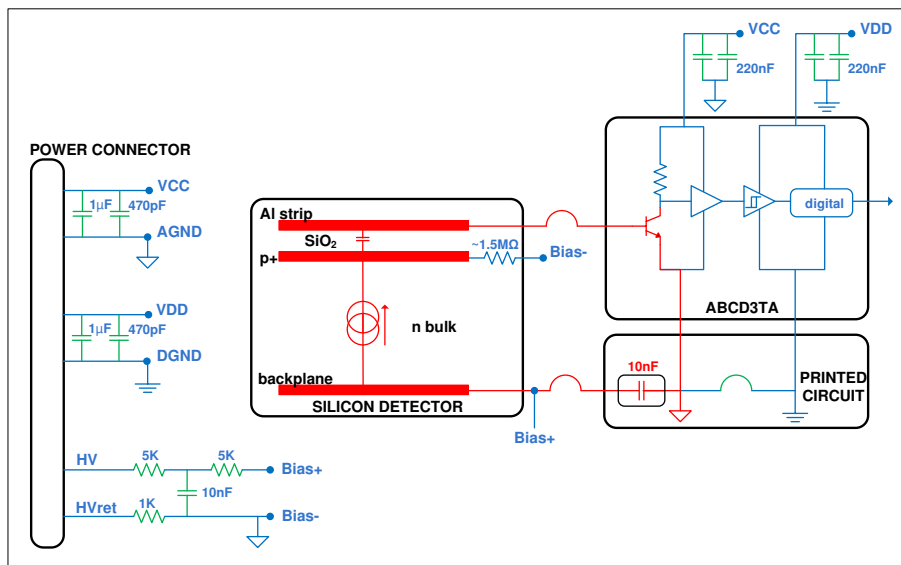
Figure 10. Module schematics. The small-signal path contains the detector, the analogue amplifier in the chip, the analogue ground (AGND) and the HV bypass capacitor. Analogue ground (AGND) and digital ground (DGND) are tied together in the printed circuit. Noise filtering is applied close to the power connector and bypass capacitors are placed close to the chip.

This section describes how the different components of the SCT affecting the grounding and shielding have been designed and implemented following the requirements indicated in the previous section. SCT grounding and shielding conforms to the proposals in references [11, 12].

4.1 Detector module

The SCT modules were described in section 1. The small-signal path is contained in the detector module, going from the silicon to the amplifier in the chips (figure 10).

Three power supply sources provide current to the module: the analogue power supply and its return that power the analogue part of the chips, the digital power supply and its return that power the digital part of the chips (pipeline, readout buffers and communication), and the silicon high voltage and its return to bias the detector.

The possible noise arriving on analogue and digital supplies is filtered by capacitors close to the power connector. In addition, four bypass capacitors are located close to each chip (two for the analogue supply and two for the digital one).

The EMI-sensitive analogue path (small-signal path) should be detached from noisy sources such as the digital circuitry. Thus, in the ABCD3TA, the analogue and digital circuits and grounds are completely independent. Only in the discriminator section is a correct reference of analogue and digital grounds needed. In order to isolate geographically this coupling and avoid noise currents entering the chip, the analogue and digital ground connection is done outside the chips in the printed circuit by means of bond wires.

The high-voltage supply has a filter network close to the power connector as well. The HV return line is referenced to the analogue ground through a 1K Ω resistor. The high-frequency signal passes through the HV-bypass capacitor to close the small-signal loop.
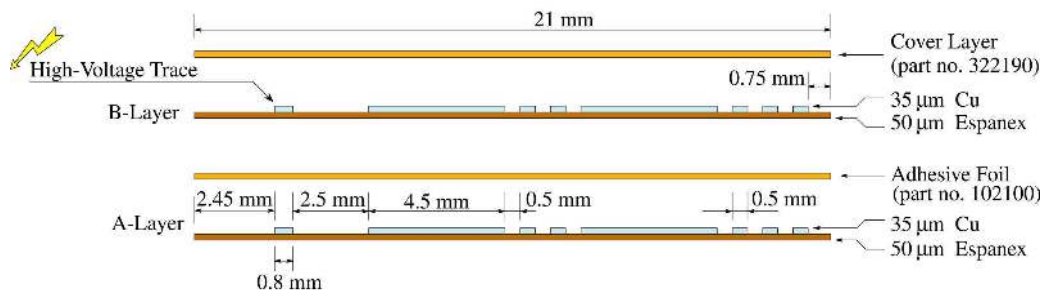
Figure 11. Cross-section of the endcap LMT with copper traces. Barrel tapes are similar, but with a $50\,\mu$m-thick layer of aluminium instead of $35\,\mu$m of copper.

Special care has been taken on the printed circuit board to provide good ground planes for analogue and digital separately. The analogue ground layer is part of the small-signal path; return currents of the digital circuits are kept away in their own digital ground layer. They provide a low impedance return to the source for noise power generated on the board; they also provide some level of shielding between circuit sections.

4.2 Low-mass tapes

As an extension of the power-supply cables, metal-on-kapton low-mass tapes (LMTs) are used inside the detector volume to carry power, sensing and control signals, and high-voltage bias to each module. Tapes in the barrel run from the modules to the first patch panel (PP1). In the endcap, very low-mass ribbon cables with twisted-pair copper-clad aluminium power wires run from the modules to a patch panel at the edge of each disc (PP0), with LMTs from there to PP1. The PP1s are just outside the respective Faraday cages.

Material in the ATLAS inner detector degrades the tracking performance as well as that of the calorimeter. The significance of material grows towards the interaction point. Thus, as tapes run inside the detector volume, they were designed to use aluminium as a conductor and are unshielded to avoid extra material. Tapes inside the barrel shield use aluminium. However, the barrel tapes were found to be fragile in the regions where the aluminium had been Ni plated for soldering. Thus, it was decided to use copper conductors for the endcap tapes [13, 14].

Tapes are constructed of two glued layers of single-sided tapes (figure 11) with a width of 21 mm and a thickness of $330\,\mu$m. Low-current lines for sensing and control have a width of 0.5 mm and high current ones for powering have a width of 4.5 mm. The high-voltage lines are 0.8 mm wide and IPC-2223 specification is obeyed for HV separation (2.5 mm for 500 V). The range of tape lengths in the barrel is 0.7-2.1 m, in the endcap 1.3-3.1 m.

Rather large currents flow through the power tapes, typically 1.7 A in each of the 4088 tapes. The tape design maximises conductivity because a significant voltage drop converts to undesirable power dissipation inside the cold volume. The resistance specification is 250 mΩ/m for the 4.5 mm power lines for the barrel and 150 mΩ/m for the endcaps. The difference arises since the endcap tapes are longer than the barrel ones. For the 0.5 mm lines, the resistivity is 2.24 Ω/m for the barrel and 1.7 Ω/m for the endcap.

In order to reduce the sensitivity to pickup noise and given that the tapes are unshielded, the power and return lines in the top and bottom layers are coupled back-to-back minimising the current-loop area. The misalignment in the top and bottom layers had to be smaller than 0.2 mm. The wide power and return lines have a capacitance of 1.9 nF/m and an inductance of 20 nH/m.

4.3 Cooling pipes

The cooling loops inside the detector volume are referenced to the SCT ground by connecting them to the shield. In order to improve the good referencing of each loop and also that between different loops, a copper disk sheet (Cooling Reference Disk - CRD) is added at both ends of the barrel. Litz wires connect each loop to the CRD. Each barrel cooling loop enters and exits the shield on the same end of the barrel [2], however, its path inside the shield takes it very close to the other end. A barrel cooling loop is referenced at both ends to both CRDs, in order to equalise the referencing of all loops independent of which side of the barrel they enter.

The endcaps have the Radial Cable Tray (RCT) structure [3], to which the cooling loops are connected. In addition, a copper-grounded foil was added for each endcap disk and soldered to the cooling pipes. This reduces the impedance to ground-loop currents.

As mentioned, the cooling loops inside the shield are referenced to SCT ground. The external metal cooling tubes, running metres along the rest of the ATLAS subsystems and from the cooling plant in the adjacent cavern, are earthed to an ATLAS ground different from the SCT ground. In order to preserve the SCT isolation, an electrical break in the cooling tubes is implemented outside the detector array shield in its vicinity.

The cooling pipes form conductive loops inside the detector volume. In addition, they run very close to the detector backplanes, being a source of noise pickup into the small-signal path.

A system test was realized during the design and test phases of the SCT construction [15]. It consisted of a barrel sector to support up to 48 modules and an endcap sector of a quarter-disk to host up to 13 modules. It used system components (cables, fibres, cooling pipes, etc.) similar to the final detector. One of the aims of the system test was to investigate the effect of pickup, crosstalk and common-mode noise as functions of module location, grounding and neighbour module configuration. Many tests were developed and it influenced the design of many of the endcap and barrel system components: power-cable routing, shielding, connections, hybrid grounding (section 4.1), etc..

When operated in a multi-module run on the system test, the SCT modules showed similar electrical performance compared to being operated individually on the bench. So, in order to test the detailed performance of each grounding and shielding configuration, noise was deliberately injected into the power tapes and cooling pipes. The best results were obtained with the module ground connected to the module cooling block [16].

Two different options of cooling-block connection were used for barrel and endcap modules. In the barrel modules, a shunt shield was used. It consists of an additional conductive layer in the module mounting-block, between the cooling tube and the detector (figure 12). The layer is directly connected to the LMT ground entry point at the module connector. Thus, the ground loop due to the cooling tube no longer includes the detector sensor and the small-signal path is protected. Most of the currents in this ground loop flow through the power tape only, leaving the sensor more
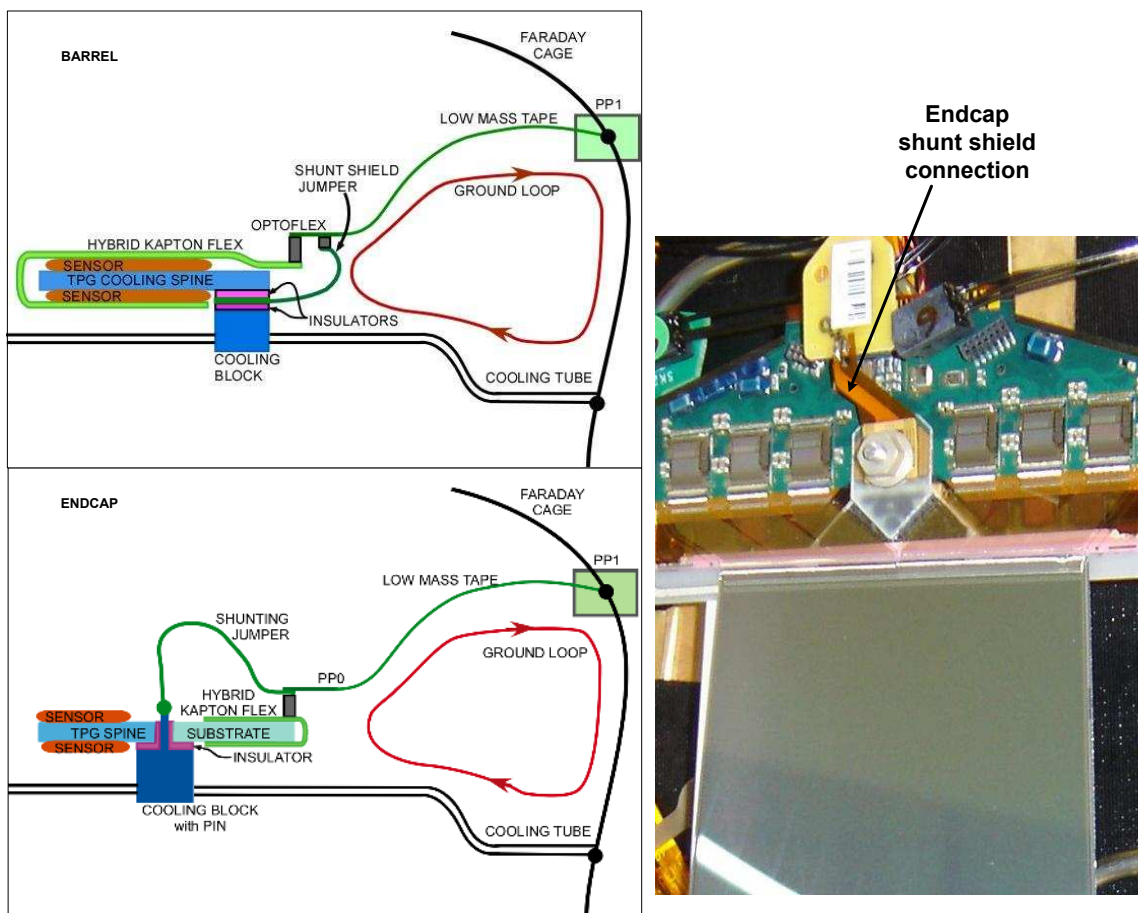
Figure 12. Shunt shield implementation. The connection to the module connector diverts noise pickup in the cooling circuit to SCT ground, keeping the noise away from the small-signal path. The picture shows the connection from the endcap cooling to the LMT power connector.

isolated from stray currents. The stray capacitance from the tube to the sensor is reduced to 1 pF or less.

With the shunt shield in place, any variation in the potential of the cooling pipe will induce current on the shield rather than the hybrid ground or detector backplane; hence the resulting signal is shunted to the module ground at the power connector.

The shunt-shield flexible circuit was used over the cooling block. To optimise the capacitive shielding, a small overhang of 1 mm was added to the shunt shield. This also had the benefit of providing extra protection against HV breakdown between the module and the cooling block. The shunt shield was made from 18 μm copper on 25 μm polyimide and was connected to the analogue ground on the electrical connector of the module [2]. The option of changing the grounding scheme to connect the cooling block to the module analogue ground was made available by a tab which could be connected to the cooling block by a screw; however, this connection was never required. The thermal impedance of the shunt shield had to be minimised in order not to increase significantly the temperature difference between the cooling block and the module. To this end, the shunt shields were attached to the cooling blocks with 20 μm of epoxy loaded with boron-nitride.

In the endcap modules, a similar solution was adopted in order to avoid the ground loop including the detector backplane or hybrid ground. System test results showed that in the endcap geometry, the best performance against noise was achieved by DC-connecting the cooling block to the power connector (figure 12).

4.4 Faraday cage

The Faraday cage is a key element in the grounding and shielding concept. It not only acts as a shield against external electromagnetic radiation, but as a low-impedance path for possible noise currents. The aim is to keep noise currents out of the detector volume defined by the cage. The cables and patch panels are referenced to the cage by low resistance connections.

The SCT has three independent subdetectors: Endcap A, Barrel and Endcap C. Each one is independently earthed and has its own Faraday cage. The SCT Faraday cage functionality is provided by the thermal enclosure. This has other functions as well as the grounding and shielding:

- It provides mechanical protection for the SCT assembly.

- It provides thermal insulation between the SCT and TRT, which operate at different temperatures, -7°C and $+25^{\circ}$C respectively.

- It contains a dry-nitrogen atmosphere to avoid condensation.

- It separates the SCT and TRT gas volumes, and also the volume between SCT and TRT that is flushed with CO_2.

- Finally, it acts as an electrically earthed shield, giving a good voltage referencing for cables and patch panels. The apertures of the shield have been kept to the strict minimum for services access.

The design was challenging, as all the above functions had to be accomplished with the constraints of minimal mass, gas tightness and a very strict mechanical tolerances defining the envelope. The barrel Faraday cage was realised in aluminium and the endcap ones in copper (figure 13).

Due to various constraints, the cages are not one piece. Significant care was taken to minimise impedance by use of gaskets, lap joints and conductive glue and implementing high-quality corrosion-proof electrical joints that will not deteriorate throughout the lifetime of the SCT. In addition, the electrical shield had to be as continuous as possible; gaps and seams were minimised. References [2, 3] explain in detail the design of the thermal enclosures.

In order to prevent corrosion in the barrel cage and avoid increased resistance across aluminium joints, all aluminium parts were treated with Alochrome 1200 to resist oxidation, thereby providing a more reliable, long-term electrical connection. In the skin design, particular attention was given to the Al-joint bonding technique, in order to reduce the AC impedances of the joints. A spot-welding technique was used to weld aluminium tabs to the outer-cylinder aluminium skin (see figure 13). During assembly, the tabs were folded over the rim and bolted to an annular copper ring. A silver-coated nickel epoxy, EP79, was used for some electrically conductive joints. Many joints included commercial tin-plated Be-Cu radio-frequency gaskets.[1]

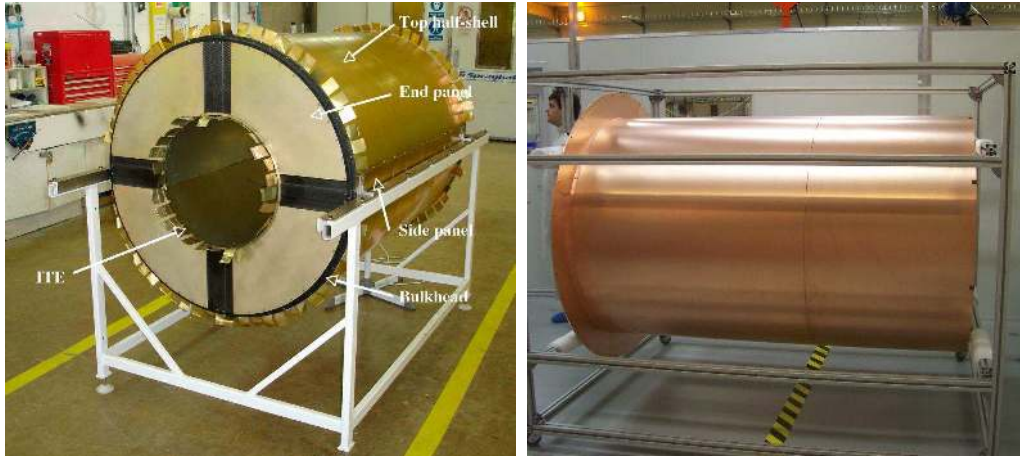[1]Laird Technologies, http://www.lairdtech.com, part number 0C98-0550-17.

Figure 13. SCT Faraday cages. The barrel one (left) was made of aluminium sheets with alochrome plating and the endcap ones of copper foil on a foam cylinder (right).
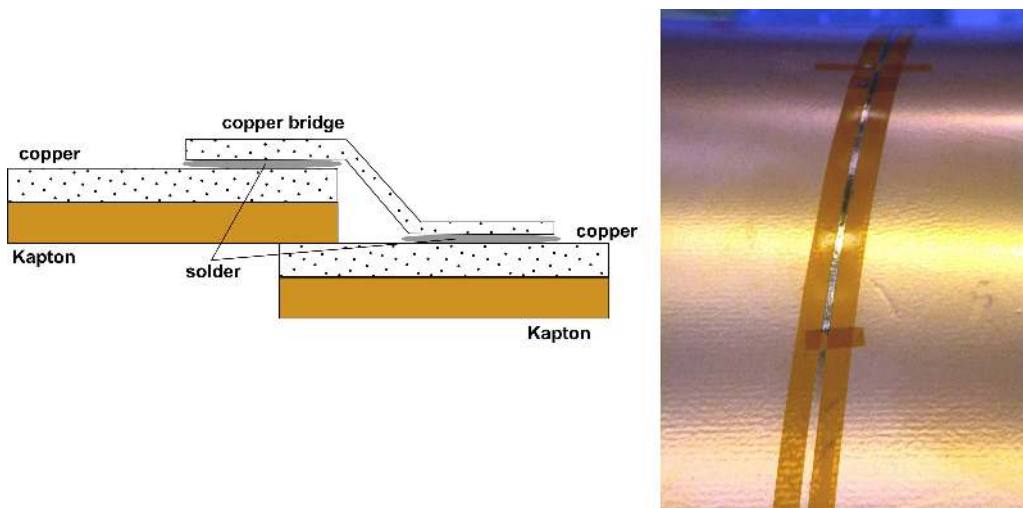

Figure 14. Diagram of the bridging solder technique (left). Right-hand figure is a picture during the soldering. Temporary tape forms a channel for controlling the extent of the solder bridging gap between the two Cu-polyimide sheets.

Reference [17] details the grounding and shielding implementation for the structure parts of the endcap. The endcap cage was formed from sheets of Cu-polyimide. Since no single sheet was big enough, several were required and were connected using a "bridging" technique illustrated in figure 14. The bridging was made with strips of copper foil 3 mm wide. To avoid handling problems associated with long strips of foil, the foil was cut into sections ∼10 cm long and joints were made with ∼1 cm gaps between two bridges (figure 14). At the Services Thermal Feed Through (STFT) at the end of the endcap, gaps allow services to pass through. An attempt was made to limit apertures to less than 1 cm x 10 cm.

To check the correct implementation of the grounding scheme, extensive measurements were made to ensure that intended connections were indeed of low resistances and no unwanted electrical

paths had been created inadvertently. DC measurements of various items used in the assembly were made in a systematic way in the SR1 surface building at CERN so that any corrective action could be undertaken before the detectors were installed in ATLAS. The connections were also monitored after installation and showed no deterioration.

Two measurement techniques were used:

- A standard multi-meter was used to measure resistance with a precision of 0.1-0.2 Ω. Since a multi-meter functions with a very small current, this method presented a low risk for devices built with semiconductors.

- A current source set with a limit of 3 A combined with a very precise voltage measurement enabled resistances to be determined down to $10\,\mu\Omega$ (impossible with the other technique).

In the barrel, the resistance across the different lap joints of the aluminium skin is typically $\sim 0.16\,\text{m}\Omega$; the resistance between the top half-cylinder and bottom half across the side panel is $\sim 0.5\,\text{m}\Omega$.

In the endcaps, the conducting paths had resistances less than $0.2\,\text{m}\Omega$; while insulating paths had resistances in excess of $1\,\text{M}\Omega$.

The three SCT subdetectors are inserted into the TRT subdetectors, which are inside the AT-LAS Liquid Argon Calorimeter and the solenoid. All these structures act as electrical shields against radiated EMI. However, the SCT Faraday cages add additional protection. The shielding effect against external EM fields is obtained by reflection and absorption of the EM wave.

As mentioned, reflection on the shield reduces the EM fields. The loss due to reflection on the shield at normal incidence is [18]:

$$A_r = 20\log\frac{|Z_w|}{4|Z_s|}[dB] \tag{4.1}$$

Z_w is the characteristic impedance in air of the EM wave and Z_s the one of the shield. Z_w in the air and for far field is $377\,\Omega$. The transition from near to far field occurs at $\lambda/2\pi$. At a frequency of 10 MHz, to which the chip amplifier is the most sensitive, the transition occurs at $\sim$5 metres. In the near field, Z_w (=E/H) is determined by the characteristics of the source and the distance.

Z_s for copper and aluminium is [18]:

$$|Z_{s,Cu}| = 3.68 \times 10^{-7}\sqrt{f} \ ; \ |Z_{s,Al}| = 4.71 \times 10^{-7}\sqrt{f} \tag{4.2}$$

At a frequency of 10 MHz and far field, the SCT Faraday cages provide a reflection shielding of 98 dB and 96 dB for the copper endcap cage and the aluminium barrel cage respectively.

The loss due to absorption through a shield is [18]:

$$A_a = 8.69\left(\frac{t}{\delta}\right)[dB] \tag{4.3}$$

where t is the thickness of the shield and δ the skin depth of the material at a given frequency. The skin depths of copper and aluminium at the most sensitive frequency are:

$$\delta = \sqrt{\frac{2}{\omega\mu\sigma}} \ ; \ \delta_{Cu,10MHz} = 20.3\,\mu m \ ; \ \delta_{Al,10MHz} = 25.4\,\mu m \tag{4.4}$$
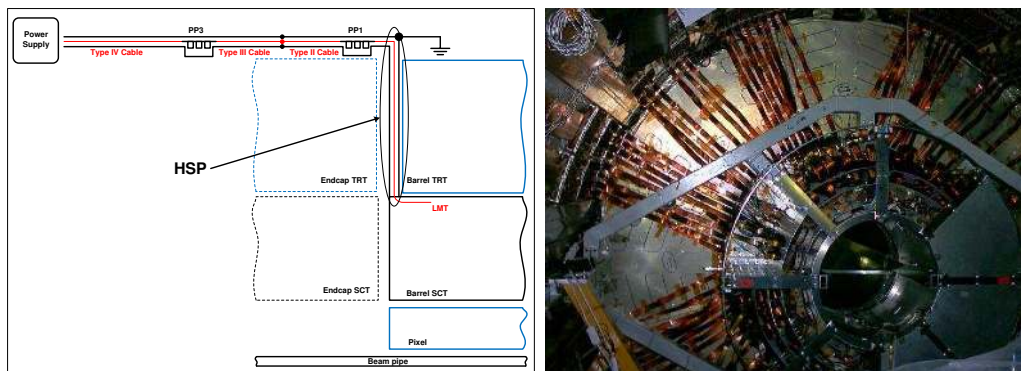
Figure 15. The HSP. The schematic shows the cross-section of the inner detector with the position of the HSP. Unshielded LMTs are protected up to PP1. The picture shows the HSP during installation when the front cover of the HSP was not yet installed and the LMTs were being routed.

where ω is the angular frequency, and μ and σ are the magnetic permeability and the electrical conductivity of the material.

The SCT barrel cage provides an absorption shielding of 171 dB for the 500 μm aluminium barrel shield. The endcap copper skin is thin (18 μm), providing little absorption protection (6 dB).[2]

4.5 Heat spreader plates and segmented plates

The Heat Spreader Plate (HSP) and the Segmented Plates (SP) are two mechanical structures of particular importance for the grounding and shielding design. Both are electrically conductive rings at the SCT cage ends providing good azimuth connection between the PP1 filters.

The HSP is a sandwich of alochromed aluminium providing shield protection to the services running out of the barrel enclosure, in particular it protects the LMTs up to the PP1 filter (figure 15).

As mentioned previously in section 3.2, cables arrive to PP1 from very different paths; therefore, a very good electrical connection to the Faraday cage is required (figure 8). The HSP is the structure that provides this connection. The bondings of the PP1 to the HSP and the barrel-shield cylinder to the HSP have received particular attention in order to have very low AC impedance. In addition, the HSP needs excellent circumferential conductivity to connect the PP1s together. These were achieved with the use of screwed metallic pieces with radiofrequency gaskets in each joint and star-serrated lock washers.

The safety-earth connection of the Faraday cage is made at the HSP; this is the unique ground tie of the barrel detector. Similarly, the safety-earth connection of each endcap cage is made at the Segmented Plates.

In the endcap, the services (LMTs, cooling pipes, fibres, temperature and humidity sensors, etc.) are routed with the help of two ring structures: the Radial Cable Tray (RCT) and the Segmented Plates (SP). PP1s are located on the SP (figure 16), so the endcap SPs are the electrical equivalent of the HSP. Good connections are needed: circumferentially between the SP parts, between the PP1 and the SP and also between the SP and the endcap cage.

---

[2]Note that for thin shields, the magnetic protection is reduced due to multiple reflections [18] by $20\log(1 - e^{-2t/\delta})[dB]$, 2.4 dB for the endcap skin.
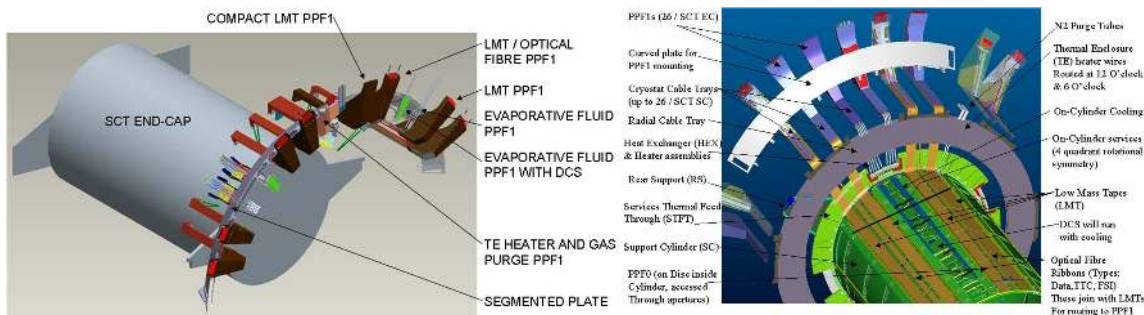
Figure 16. The Segmented Plates. Schematics showing one half of the PP1 patch panels.
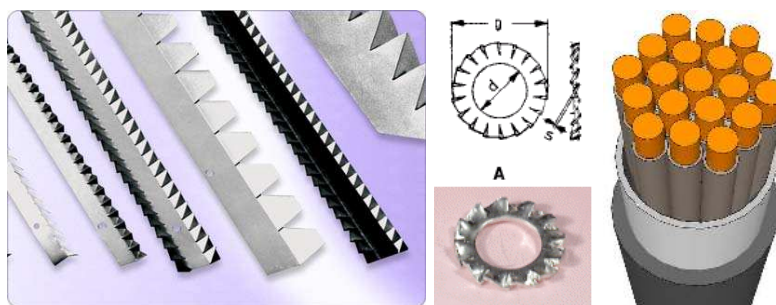

Figure 17. EMI fingerstock gasket (left) and star-serrated lock washers (centre) penetrate the metal. Litz wire (right) consists of multiple strands insulated electrically from each other. Ordinarily the strands are twisted or woven, but no twisting is shown in this diagram.

Each one of these connections, barrel and endcap, used EMI fingerstock gaskets and star-serrated lock washers (figure 17) on every screw, ensuring penetration of surface oxide layers and the alochrome. In addition, Litz wires were used to reduce the skin effect between critical pieces (some Segmented Plates, the cooling reference disk and others).

The inner detector subsystems (Pixel, SCT and TRT) are located inside a solenoid field of 2 Tesla. In the case of a solenoid quench, the longitudinal field would collapse and induce electromagnetic fields in closed circuits in which the flux changes. These fields would induce currents which could damage sensitive electrical components; or produce forces in the conductors which could damage them or exert significant forces on the SCT and surrounding structures.

The consequences of a solenoid quench were thoroughly studied [19]. Calculations predict high forces (∼1000 N) on the Radial Cable Tray, which is a closed low-resistance annulus. Although the structure should withstand these forces, it was decided to break the connection in one azimuthal position. The RCT has two annuli (Front and Rear) sandwiching the radial services. An insulating sheet was used for the Front RCT, whereas a capacitive flex circuit was used for the Rear RCT, so that good circumferential conductivity against noise currents is kept.

All conducting material of the barrel and endcaps was grounded. This includes the carbon fibre structures of the barrels and disks. Carbon-loaded plastic fittings were avoided to simplify the grounding requirements.

The three inner detector subsystems are grounded at a controlled location, identified as IDGND. IDGND is a star connection of all safety grounding cables for the inner detector subde-
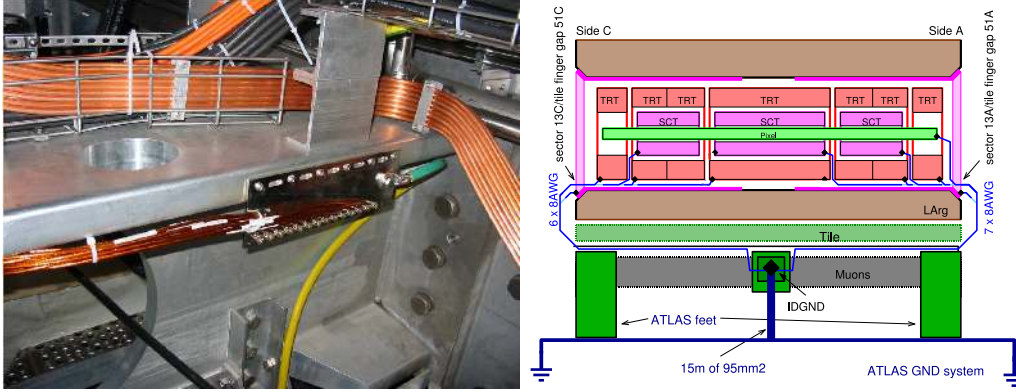
Figure 18. IDGND star point for the ID subsystems. The schematic on the right shows the routing of the earth cables, for the SCT and TRT barrels one cable was routed on each side, but only one is connected to the Faraday cage (side A is connected for SCT barrel and side C is connected for the TRT barrel).
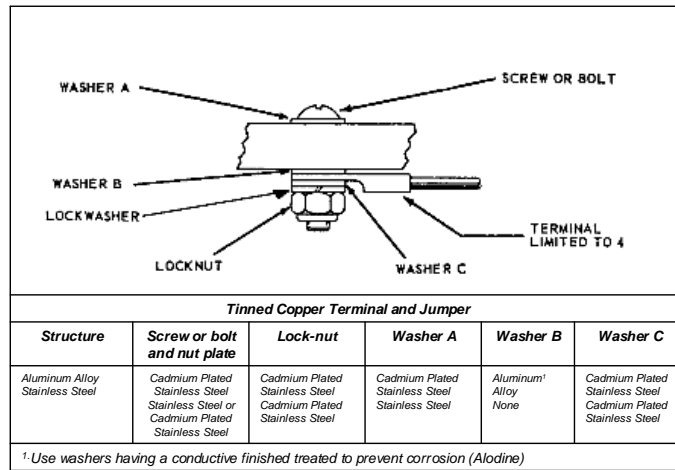

	Tinned Copper Terminal and Jumper				
Structure	*Screw or bolt and nut plate*	*Lock-nut*	*Washer A*	*Washer B*	*Washer C*
Aluminum Alloy Stainless Steel	*Cadmium Plated Stainless Steel Stainless Steel or Cadmium Plated Stainless Steel*	*Cadmium Plated Stainless Steel Cadmium Plated Stainless Steel*	*Cadmium Plated Stainless Steel Stainless Steel*	*Aluminum[1] Alloy None*	*Cadmium Plated Stainless Steel Cadmium Plated Stainless Steel*
[1]Use washers having a conductive finished treated to prevent corrosion (Alodine)					

Figure 19. Bolt and nut bonding or grounding to a flat surface (ref. [21]).

tectors. The IDGND point is connected to ATLAS ground (figure 18). The star configuration minimises the potential differences between subdetectors, so reducing possible noise currents through stray capacitances.

The three SCT safety earth cables going from the Faraday cages to the IDGND point are single core AWG 8 119/0.3 mm protected with kapton/polyimide foil. The same type of cable is used for the rest of the Inner Detector subsystems (pixels and barrel and endcap TRTs).

Given the importance of the unique safety-earth connection to the Faraday cage, the specification AC43.13-1B document by Federal Aviation Administration for grounding in the aircraft has been followed for reliable aluminium-to-copper bonds [20, 21] (figure 19).

4.6 Power cables

The power supply for the front-end electronics (analogue and digital), the high-voltage supply for the silicon detectors and other control lines are delivered to each of the 4088 SCT modules
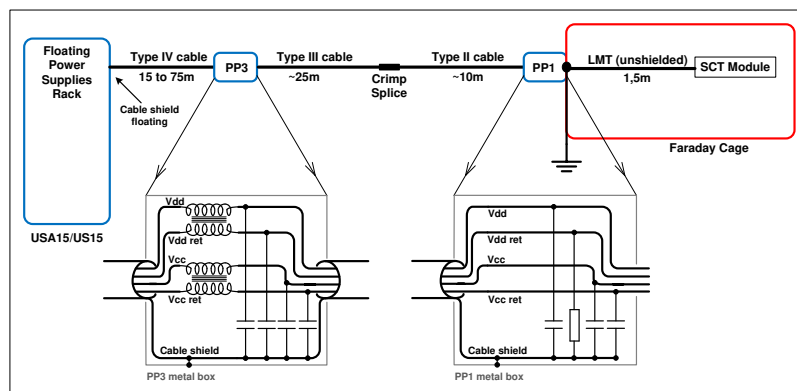
Figure 20. SCT power supply cable description.

with a foil-shielded cable, consisting of 16 insulated conductors [22]. An uninsulated drain wire supplements the aluminium-foil shield. The drain wire is in contact with the shield all along the cable length. It ensures the connectivity of the shield between both cable ends.

Minimising the service material inside the detector and keeping the detector as hermetic as possible led to the use of thin cables that have higher resistance. Also, having long cables contributes to higher resistance, as well as to increasing the noise sensitivity.

The cables have two mechanical connector locations mandated by the mechanics assembly. These are referred to as patch panels PP1 and PP3. Both provide a noise-filter function and are a transition between two cable sizes. PP1 is a PCB located close to the detector array shield and the PP3 PCB is located ∼35 m from the detector. As mentioned, space for services is restricted in the region where the services converge on the detector volume. In order to minimise resistance in the very restricted service volume, there are four types of module cables, with different types of connections between them (figure 20):

- Type IV: cable up to 75 m between the power supplies and PP3. It has large cross-section and straight conductors to save volume.

- PP3 provides cable connection and has noise filters with a bypass capacitor and common-mode ferrite choke on each conductor. EMI sources on Type IV cable are largely attenuated by the common mode chokes. The choke array allows the bulky Type IV cable to have straight pairs, reducing the cross-sectional area by 30%.

- Type III: cable (∼25 m) between PP3 and Type II cable. It has a moderate cross-section and twisted pair conductors to reduce magnetic EMI across supply pairs.

- A crimp splice at each conductor provides connection between Type III and Type II cables.

- Type II: cable (∼10 m) between Type III cable and PP1. It has a minimum cross-section, hence the thick conductors are insulated with kapton. Special twisted groups have been used to optimize cross-section versus magnetic rejection.

Table 1. Power supply cable sizes and resistances. The resistances correspond to measured values on final cables. The resistance value of the drain wire includes resistance of the shield as they are in close contact.

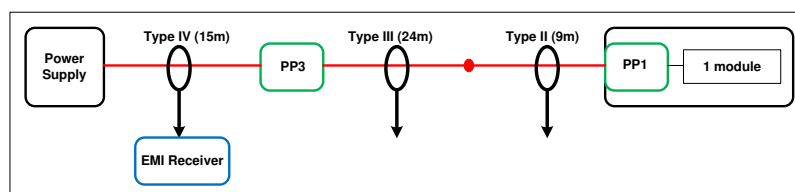|	Type IV cable		Type III cable		Type II cable	
	Size(mm^2)	R(mΩ/m)	Size(mm^2)	R(mΩ/m)	Size(mm^2)	R(mΩ/m)
Power	4.00	4.6	1.00	21.2	0.518	32
Control	0.25	72.5	0.14	136	0.081	206
HV	0.14	137	0.14	136	0.081	206
Drain Wire	0.75	9	0.75	12.8	0.205	61

Figure 21. Test setup for the conducted emissions measurement.

- PP1 provides cable connection at the Faraday cage. It incorporates a simple bypass-capacitor filter on each cable conductor. In this way, all conductors going inside the shield short to the Faraday cage or equivalently have a capacitor bypassing.

- Type I: low-mass tapes (described in detail in section 4.2).

Table 1 summarises sizes and resistances for each conductor.

Power-supply cables were tested in the laboratory to measure their conducted electromagnetic emissions. The setup arrangement is shown in figure 21. The test used production components that were being installed in ATLAS: power supply, cables and patch panels.

Results showed that SCT cables were emitting well below ATLAS limits, with the exception of some points around 300 KHz (figure 22). The effect of PP3 is clearly seen, achieving a good attenuation in the important range of 1-20 MHz. Noise is slightly worse on Type II cable. The cable shield at the power supply is left floating, as already mentioned. Grounding the shield at the power supply (see figure 23) reduces the emission in the 150-600 KHz range, but it increases the emissions in the 1-2 MHz range. During the installation the shield was left floating at the power supply, following ATLAS guidelines and avoiding ground loops. However, if noise deteriorates in the future, a special card has been installed in the power supply rack, which provides a fast and easy way to ground the shield at the power supply. Measurements after the full ATLAS installation and operation have not indicated any noise problem.

The digital transmission lines to and from each of the SCT modules are served with optical fibres [23]. The choice of optical fibre as the physical media has many advantages: the much smaller cable size and, in the scope of the grounding and shielding design, its immunity to electromagnetic interferences, its exceptionally low loss (no repeaters are needed) and the absence of ground currents or other parasitic signals.
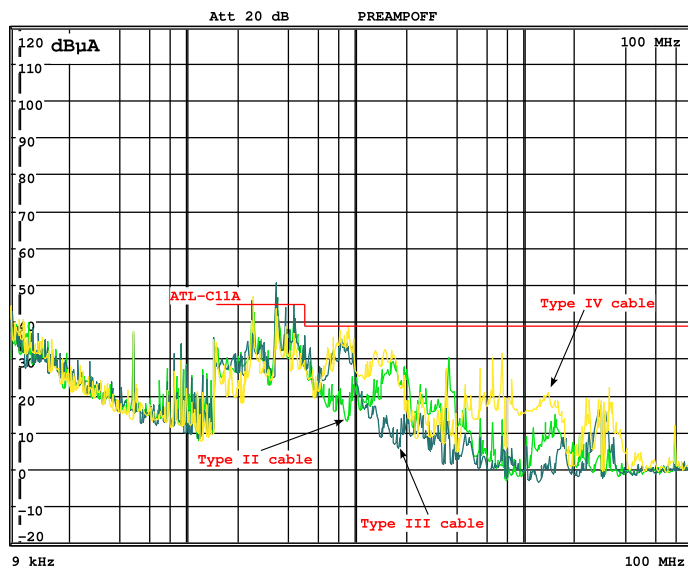
Figure 22. Emissions from the three cable types. Module is powered, configured and data is read out during the test. Type IV cable emissions are reduced after PP3. Noise increases slightly on Type II cable.
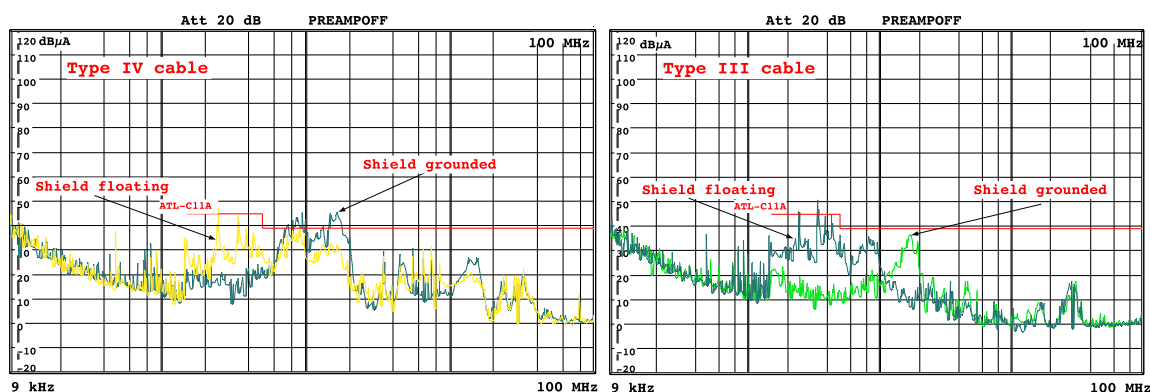

Figure 23. Comparison of grounding or not the shield at the power supply. Plots show emissions from Type IV and Type III cables.

4.7 Patch panels

Patch panels (PP3 and PP1) have been already introduced in previous sections. In addition to the electrical functions, they have the mechanical function of interfacing two cable types: PP3 interfaces Type IV and Type III cables and PP1 interfaces Type II and the LMTs. The LMTs are soldered on the PP1 PCB. PP3 is located in a dedicated rack at the outer edge of the ATLAS detector cavern (UX15). Barrel PP1s are located on the cryostat wall close to the HSP. The endcap PP1s are located on the SPs. All have an electrical housing as indicated on figure 20.

PP3s are individual isolated units; there is one per module. As already mentioned, they have common-mode inductive filters on all lines, both power and control, to attenuate any common-mode noise that may be picked up on the long run of Type IV cable. In addition, every conductor is bypassed through a capacitor to the cable shield. The drain wire is routed on the PCB providing

Figure 24. PP3 pictures. Top view with metal box open (top), the yellow wire connects the metal box to the cable shield. Front view of the PP3 (bottom), the two C-section pieces protect against magnetic fields. PP3 rack before cable installation (right).

continuity of the cable shield from Type IV to Type III cable shield. The metal box and the cable screens are electrically isolated to avoid contact with any other PP3 and all surrounding structures by means of fibre-glass sheets. A wire connects the metal box to the cable shield.

The location of the PP3s inside UX15 is exposed to fringing magnetic field of the ATLAS barrel toroids. Simulated field maps indicate that up to 600 Gauss may be present. The inductive chokes used to attenuate common-mode pickup saturate at external fields around 100-200 G. The metal box is designed as a magnetic shield, and additionally acts as electrostatic shield. Different materials and configurations were tested. The best results (25 G inside the box with an external field of 800 G) were obtained with a box material fabricated from sheets of 0.5 mm thick grain-oriented silicon transformer steel. Two C-section pieces are spot-welded together to form a rectangular cylinder (figure 24). The PP3 boxes enclose the cable connectors as well as the circuit board along their whole length.

PP1s (figure 25) are printed circuits accepting low-mass tapes from the detector side and conventional cables from the power-supply side. Barrel PP1s serve 6 modules, whereas endcap ones have two flavours: one serves two modules and the other three modules. Every conductor is AC coupled to the Faraday cage before entering the cage by means of a capacitor. The shield of the cable is connected to the PP1 metal enclosure. The PP1 enclosure is connected to the Faraday cage and the safety-earth cable. PP1s also provide AC coupling of analogue, digital and HV power lines to their return lines.

In the barrel, the cable shield and the metal enclosure are connected to the digital return line (DGND). The barrel SCT modules are grounded at PP1; the analogue and HV return are referenced to the digital return in the module (section 4.1). In the endcap, the modules are referenced at a small PCB called PP0 on the disks, very close to the modules. At PP0, the DGND line is connected to the Faraday cage. The referencing of the power returns in the SCT is represented in figure 26.
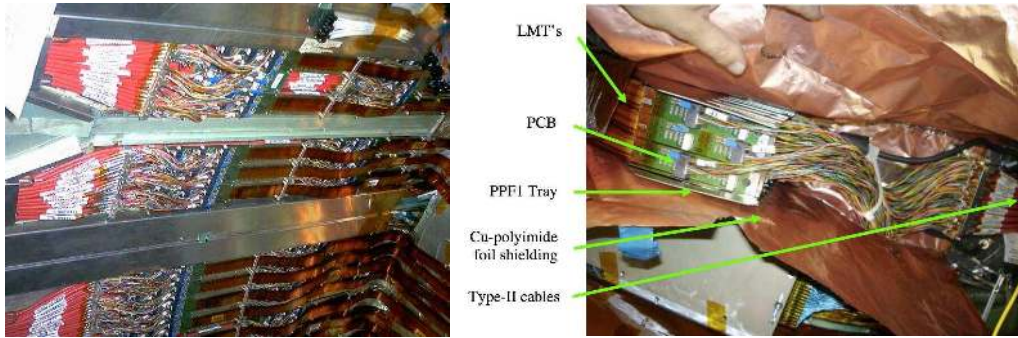
Figure 25. Barrel PP1s without the cover (left), with Type II cables (red) and LMT connected. Endcap PP1 (right) with the electrical housing opened.
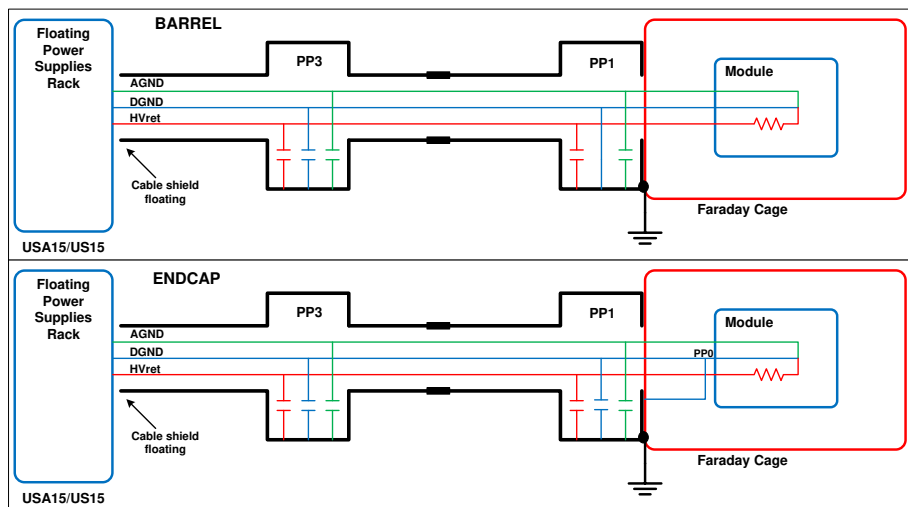

Figure 26. Referencing of the SCT power returns.

4.8 Power supplies

The SCT power-supply system [24] consists of several components located in adjacent caverns USA15 and US15. Regarding grounding and shielding, the main point is that the different power supplies must be floating. The isolation of individual channels and individual voltages is realised by HF transformers on the power path and by optical couplers on communication lines. As mentioned, the Type IV cable shield is left floating at the power-supply side. In this manner, any DC ground loop is avoided.

The final grounding and shielding implementation could only be tested after full installation. Thus, an additional card in the power-supply system has been added. A shorting card allows us to easily ground the Type IV cable shields. This card is unconnected but is kept in case of future problems.

4.9 Other systems connected to SCT ground

There are other mechanical and electrical systems connected to SCT ground. The mechanical systems (CO_2 and nitrogen pipes, metallic structures, etc.) were carefully controlled to not short to
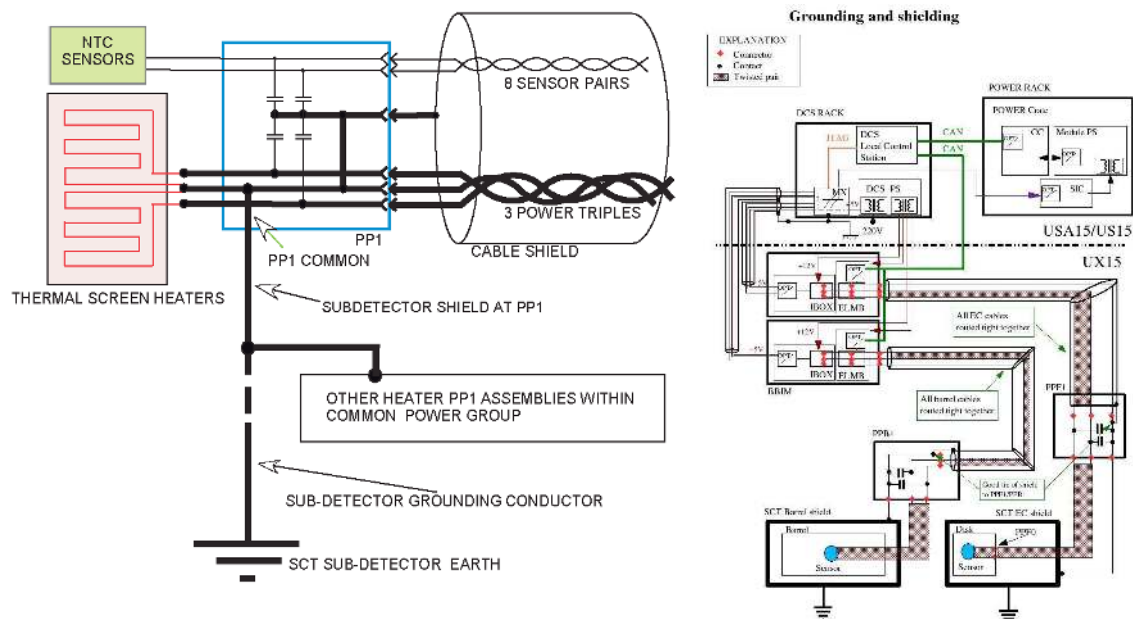
Figure 27. Grounding of the heater control system (left) and the environment monitor and control system (right).

any other subdetector, keeping the SCT referenced with a single tie.

Other electrical systems, including the large area heater pads and the environmental control (temperature and humidity sensors), are connected to the SCT ground. The heater pads are used to maintain the interface between various subdetectors at a predefined temperature. Special care has been taken to maintain the electrical isolation of these systems. Figure 27 describes the grounding of the heater and environment control systems.

The grounding of the heater system follows the same rules as the SCT power-supply system. It is grounded to the Faraday cage at PP1, the power supply is floating and the cable shield is only connected at the detector end [20]. The same principle applies to the environment control system; in addition, all signals are isolated by optocouplers.

4.10 Ground isolation monitoring during installation

The installation of the three SCT subdetectors, the power-supply cables, the optical fibres, the patch panels, the cooling pipes and other components was a very difficult task that took several years. Furthermore, the space in the inner detector is very restricted and the different subdetectors and their services have very little clearance between them. As a consequence of this, it was very easy to accidentally short a part of one subdetector to a part of another one, violating subdetector isolation and single earthing. Even with a periodic check of the isolation, in a very big system like the SCT it was impractical to stop all activities to look for the accidental short. Furthermore, the success in searching for a short was not guaranteed in such a big system; several people working at the same time in very different locations can easily produce multiple shorts. Finding of a multiple short is extremely difficult.
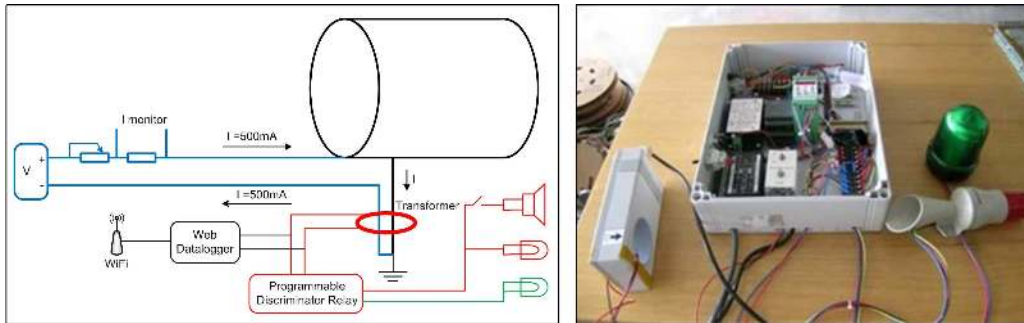
Figure 28. Ground Isolation Monitor. The transformer monitored the differential DC current. The programmable discriminator relay activated the green or red light and the audible alarm. The audible alarm had a manual switch to cut the sound in the case of a prolonged fault. The web datalogger registered the differential current each minute and sent email and SMS alerts.

A ground isolation monitor (figure 28) was developed to detect an unintentional earth fault path. The monitor was connected to a visual and audible alarm. The intention of it was to warn immediately the installation person of a fault, and thus avoid the pile up of faults. People working in the installation were trained to stop their activity when this alarm arose. For faults longer than two minutes an email and SMS text was sent to the grounding expert.

The Bergoz IPCT (Integrated Parametric Current Transformer) is the core device in the monitor. It allows the safety-earth bonding to be maintained during the continuous monitoring. A test current (500 mA) was injected into the SCT subdetector. The path for the reference current was expected to be entirely in the safety earth conductor. The return path was through a dedicated conductor. The safety earth conductor and the return path are threaded through the transformer. In the absence of a fault, all current is flowing to the ground point and returning back. If part of the 500 mA current was diverted through a fault path from the SCT to earth, the monitor detected the event. The threshold limit to trigger the alarm was set to 1 mA difference. For the SCT configuration, the monitor could detect fault paths with resistances lower than 1 kΩ.

Three monitor systems were built and installed to monitor both SCT endcaps and the barrel. They were active for several years up to the ATLAS cavern closing. The monitors can not be kept in place during ATLAS operation as the magnetic fields would saturate the transformer and render it inoperable, regardless of the possible non-resistance to radiation of its components. In August 2008, they were removed before first LHC operation. At the time of removal, the three SCT subdetectors were checked to be isolated (over MΩ or over limit in the measuring device) and earthed only in a single tie.

5 Problems and installation experience

Obviously, the design and installation phases were not free of problems. The space between services of different subdetectors was very tight (figure 4, for example). A short summary is given below listing some of the problems encountered in maintaining the electrical isolation during installation:

- Minor problems directly solved by the installation person. The ground monitor showed its effectiveness with this type of fault. There were several each day, such as installing a pipe slightly out of its position shorting to another subdetector service.

- Problems on the SCT Barrel:

  - A copper-kapton foil protects the barrel services. The edge of the foil had some exposed copper which touched TRT grounded components. The foil edge was protected with flexible kapton tape.

  - The HSP had aluminium tabs connecting to the PP1 base plate to ensure good electrical conductivity between the HSP and the PP1. The back face of the tabs was not insulated and produced multiple shorts to the Liquid Argon cryostat. They were protected with glass fibre or kapton tape.

  - The SCT cooling pipes outside the enclosure and before the electrical break were routed in a cable tray. They were electrically protected with thermal foam. However, in some points the pipes were exposed and they were shorting to the cable tray, which is connected to the cryostat ground. Extra foam protection was added.

- Problems on the SCT Endcaps:

  - Following the reception of the endcaps from Liverpool and NIKHEF, it was found that pipe brackets on the support cylinder were floating; therefore connections to the ground sheet were made. To ensure the isolation of the SCT from the TRT rails, the carbon-loaded PEEK inserts in the support mechanisms had to be replaced by unloaded PEEK ones.

  - During the insertion of SCT Endcap C into the TRT endcap, a short via the RCT (Radial Cable Tray) was detected. This was cured by adding a 200 μm sheet of G10 glass fibre to the RCT surface. The same precaution was taken for Endcap A.

  - PP1 boxes were protected with copper/kapton foil. SCT PP1s were located very tightly between TRT PP1s. The kapton foil was easily scratched by the TRT PP1 boxes installation producing a fault. The SCT boxes were additionally protected with glass fibre sheets.

  - The electrical break of some cooling tubes was shorting. They had to be replaced.

- After the insertion of Endcap C into ATLAS, a connection of 2 KΩ between the SCT Endcap C and the SCT Barrel was detected. The short was between one of the front support mechanisms and the SCT Barrel. By inserting a long (2 m) endoscope between the cryostat and the endcap (figure 29), it was found that the short was due to a CO_2 pipe. A two-metre-long extender arm with G10 glass fibre at the end was inserted into the region. The G10 was carefully placed between the endcap foot and the pipe; then the G10 and the arm were separated leaving the G10 sheet as insulation between the two subsystems.

The experience shows that the grounding and shielding system needs to put together people from different disciplines. On one side, electronic engineers, who are not necessarily experts in

Figure 29. Short before any intervention (left). G10 being inserted between the endcap foot and the barrel pipe (centre). G10 inserted (right) and separated from the extender arm (with blue tape).

material properties and mechanical structures, provide the concept design; while mechanical engineers have to design many structures affecting the grounding and shielding system implementation, and they are not necessarily experts in electronics. In addition, many technicians are involved with pieces of the grounding and shielding system during the installation of a detector like the SCT. Very good communication among people involved is crucial to achieve a successful system. This communication should start from the beginning in the design of the mechanical structures.

6 Conclusions

A great deal of effort has been made to design and implement a good grounding and shielding system for the SCT. The prevention of electromagnetic interference and noise pickup through power lines has been an important design aspect as they are the dominant noise source jeopardising electrical performance. In accordance with ATLAS grounding rules, the design accomplishes the avoidance of ground loops and the isolation of the different subdetectors. Noise protection of the most sensitive part, the small-signal path, has been pivotal. Protection has been developed against the various noise sources: noise from circuits generated locally at the module or from adjacent modules, electromagnetic radiation from surrounding detectors, currents coming through ground loops, mainly through power cables, and noise from cooling loops inside the Faraday cage.

The implementation of the grounding and shielding design has been followed during the construction and installation of the SCT. Special attention has been given to the electrical properties of materials and joints. A ground isolation monitor was installed to help during the installation. Repairs have permitted a final good implementation of the grounding and shielding system.

In order to keep good electrical performance, noise pickup in the SCT should not increase dramatically the single-module noise. Joining more than four thousand modules together was the challenge for the grounding and shielding system. Moreover, the SCT is part of ATLAS and its different subdetector electronic systems. Noise pickup on the SCT from other electronic systems had to be avoided.

The noise was measured at different stages of the SCT construction. Table 2 shows the values of the average measured noise for the barrel modules and the different types of endcap modules (outer, middle and inner). References [1–5, 25] report noise figures for single module tests, module tests on single barrel layer or single endcap disk, module tests with the full barrel or endcap and finally module tests in ATLAS. Noise increase after installation is not significant; variations are

Table 2. Average noise measured in equivalent noise charge at the input (electrons) corrected to 0^oC at four subsequent stages of integration.

	Barrel Module Noise(e$^-$,±60)	Endcap Outer Module Noise(e$^-$,±60)	Endcap Middle Module Noise(e$^-$,±60)	Endcap Inner Module Noise(e$^-$,±60)
Single Module	1470	1515	1464	1060
Single layer/disk	1480	1591	1527	1069
Full barrel/endcap with TRT	1512	1522	1551	1105
SCT in ATLAS (Dec. 2008)	1494	1593	1517	1032

well within the measurement uncertainties. In any case, it is far below the limit mentioned in section 1 ($50\,aC = 312\,e^-$). In conclusion, a good SCT grounding and shielding system has been implemented and protects the SCT from noise pickup.

Acknowledgements

References

[1] ATLAS collaboration, *The ATLAS experiment at the CERN Large Hadron Collider*, 2008 *JINST* **3** S08003.

[2] A. Abdesselam et al., *The integration and engineering of the ATLAS SemiConductor Tracker barrel*, 2008 *JINST* **3** P10006.

[3] A. Abdesselam et al., *Engineering for the ATLAS SemiConductor Tracker (SCT) end-cap*, 2008 *JINST* **3** P05002.

[4] A. Abdesselam et al., *The barrel modules of the ATLAS semiconductor tracker*, *Nucl. Instrum. Meth.* **A 568** (2006) 642.

[5] ATLAS collaboration, A. Abdesselam et al., *The ATLAS semiconductor tracker end-cap module*, *Nucl. Instrum. Meth.* **A 575** (2007) 353.

[6] A. Ahmad et al., *The Silicon microstrip sensors of the ATLAS semiconductor tracker*, *Nucl. Instrum. Meth.* **A 578** (2007) 98.

[7] F. Campabadal et al., *Design and performance of the ABCD3TA ASIC for readout of silicon strip detectors in the ATLAS semiconductor tracker*, *Nucl. Instrum. Meth.* **A 552** (2005) 292.

[8] H. Williams, *ATLAS policy on grounding and power distribution*, ATC-GE-ER-0001.

[9] G. Blanchot, *ATLAS EMC policy*, ATL-ELEC-PUB-2007-003.

[10] S. Haywood, *Module Overlaps in the SCT and Pixels*, ATL-INDET-2002-016 (2002).

[11] V. Radeka, *Shielding and grounding in large detectors*, in proceedings of *4th Workshop on Electronics for LHC Experiments*, Rome, CERN/LHCC/98-36 (1998) 14-18.

[12] M. Johnson, *Grounding and shielding techniques for large scale Experiments*, in proceedings of *8th Workshop on Electronics for LHC Experiments*, Colmar (2002) 44-49.

[13] V. Cindro and M. Mikuz, *ATLAS SCT low mass tapes*, ATLAS-IC-ES-0076.

[14] V. Cindro and M. Mikuz, *Technical specifications of Cu low mass tapes*, ATLAS-IC-ES-0103.

[15] P. Phillips, *System performance of ATLAS SCT detector modules*, in proceedings of *8th Workshop on Electronics for LHC Experiments*, Colmar (2002) 100-104.

[16] R. Bates, *ATLAS SCT endcap module and system test performance*, *IEEE Nucl. Sci. Symp. Conf.* **2** (2003) 908.

[17] S. Haywood, *ATLAS SCT end-cap grounding and shielding, engineering implementation*, ATLAS-IS-EN-0014.

[18] H. Ott, *Noise reduction techniques in electronic systems*, John Wiley & Sons (1976).

[19] S. Haywood, *Effect of solenoid quench on SCT*, ATLAS-IS-ER-0065.

[20] J. Kaplon, *ATLAS inner detector grounding and shielding, engineering implementation*, ATLAS-IC-ES-0011.

[21] Department of Transportation, *Acceptable methods, techniques, and practices - Aircraft inspection and repair*, US Federal Aviation Administration *AC 43.13-1B* (2001), http://rgl.faa.gov/.

[22] P. Wells, *Specifications of SCT power cables, type II, III and IV*, ATLAS-IC-CD-0001.

[23] A. Abdesselam et al., *The optical links of the ATLAS SemiConductor tracker*, 2007 *JINST* **2** P09003.

[24] J. Bohm, *Power supply and power distribution system for the ATLAS silicon strip detectors*, in proceedings of *7th Workshop on Electronics for LHC Experiments*, Stockholm (2001) 363-367.

[25] N. Barlow, *Operation of the ATLAS semiconductor tracker*, in proceedings of *9th International Conference on Large Scale Applications*, 30 September–2 October (2009), Florence Italy, PoS(RD09)004.